Journal of Cluster Science (2024) 35:1719–1730
https://doi.org/10.1007/s10876-024-02618-9

The Methylurolithin A-loaded PLGA-Folate-Chitosan Nanoparticles (Mu-PFCNPs), as the novel safe selective anti-colon cancer drug delivery system

Alaa Jiheel Zkaim Alhazami[1] · Vahid Pouresmaeil[2] · Masoud Homayouni Tabrizi[3]

Received: 9 January 2024 / Accepted: 28 March 2024 / Published online: 14 April 2024

Abstract

The synthesis of a targeted natural anticancer substitution has opened up a promising horizon by increasing the effectiveness of the treatment and reducing its undesirable side effects. However, the weak bio-accessibility and chemical instability of the medicinal plant phytochemicals are their main limitations. The nanospheres of poly lactic-*co*-glycolic acid (PLGA) is known to be safe due to its bioavailability and biodegradable profile. In the current study, Methylurolitin-A (MUA) was loaded into PLGA nanoparticles with folic acid-linked chitosan to investigate its antioxidant, anti-angiogenic, and anticancer activities. The MUA-loaded PLGA-folate-chitosan nanoparticles (Mu-PFCNPs) were synthesized and characterized by DLS, Zeta potential, FTIR, and FESEM. The Mu-PFCNPs' antioxidant activity was analyzed by ABTS, DPPH, and FRAP assays followed by measuring the antioxidant gene expression. Moreover, the anti-angiogenic potential of the nanoparticles was evaluated on HT-29 cells by CAM assay, conducting the VEGF/VEGFR gene expression measurement. Finally, the Mu-PFCNP selective toxicity was studied on the HT-29, A2780, PANC, and HepG2 cancer cell lines utilizing MTT assay. The nanoparticles (+30.14mV, 134nm) exhibited potent antioxidant activity and overexpressed SOD and Catalase genes in treated HT-29 cells. Mu-PFCNPs down regulated VEGF and VEGFR gene expression on HT-29 cells. Additionally, the CAM results verified the activity by indicating the reduction in the number of blood vessels. Finally, Mu-PFCNPs induced a significant selective cytotoxic impact on HT-29 cancer cells compared to other cancer cell lines. The antioxidant, anti-angiogenic and therefore anti-colon cancer activities of Mu-PFCNPs make them a suitable targeted anti-cancer compound, particularly for the treatment of human colon cancer.

Keywords MUA-loaded PLGA-folate-chitosan Nanoparticles (Mu-PFCNPs) · Antioxidant Activity · Anti-Angiogenic · Selective Toxicity · Anti-Colon Cancer

Nomenclature

PLGA	Poly lactic-*co*-glycolic acid
MUA	Methylurolitin-A
Mu-PFCNPs	MuA-loaded folate-chitosan nanoparticles
DLS	Dynamic Light Scattering
FESEM	Field emission scanning electron microscope
FTIR	Fourier transform infrared
MTT	3-(4,5-Dimethylthiazol-2-yl)-2,5-diphenyltetrazolium bromide
RTqPCT	Real-time polymerase chain reaction
ABTS	2,2-Azinobis (3-ethylbenzothiazoline-6-sulfonic acid)
DPPH	2,2-Diphenyl-1-picrylhydrazyl
FRAP	Fluorescence recovery after photobleaching
PDI	Polydispersity Index
HepG2	Liver cancer cell lines
PANC	Pancreatic cancer cell lines
HT-29	Colon cancer cell lines
A2780	Ovarian cancer cell lines
A549	Adenocarcinomic alveolar basal epithelial cell lines

✉ Vahid Pouresmaeil
vahidpouresmail@yahoo.fr; pouresmaeil.v@iaumshms.ac.ir

[1] Department of Biology, Science and Research branch, Islamic Azad University, Tehran, Iran

[2] Department of Biochemistry, Faculty of Medicine, Mashhad Medical Sciences, Islamic Azad University, Mashhad, Iran

[3] Department of Biology, Mashhad Branch, Islamic Azad University, Mashhad, Iran

HUVEC	Human umbilical vein endothelial cell lines
VEGF	Vascular endothelial growth factor
VEGF-R	Vascular endothelial growth factor receptor
CAM	Chicken Egg Chorioallantoic Membrane
EPR	Enhanced permeation and retention
EE	Encapsulation efficiency
EDC	1-Ethyl-3-(3-dimethylaminopropyl) carbodiimide
NHS	N-Hydroxysuccinimide

Introduction

Cancer exhibits a wide range of clinical symptoms, which leads to people's death worldwide. Cancer development is the complex biochemical process disrupting the cell cycle checkpoints, which are responsible for controlling the cell genomic health and proliferation rate [1, 2].

Among the most lethal human cancers, lung and colon cancers have contributed to 27.3 % of the total cancer death in 2020 [3]. Also, the pancreas [4], liver[5], and ovarian [6] cancer mortality have been reported at 77,215, 830,200, and 198,412 deaths, respectively. The cancer migration to several secondary metastatic niches is reported for both colon and lung primary cancers, which causes unstoppable cancer progression and poor quality of the patient's life [7–10].

The accelerated cancer cell proliferation and its colony development process require a dynamic progressive growth of the cell-feeding roots by forming complex alternative blood capillary nets around the growing solid tumor [11]. On the other hand, the increased input of energetic and carbonic sources such as folic acid is required to be supplied for DNA polymerization process by up-regulating the membrane folate receptors, which have overexpressed in several types of human cancers such as breast, colon, lung, liver, ovarian, pancreas cancer cells [12–15].

The high-rate produced ROS in the growing tumor mass induces the angiogenesis process and must be removed by the newborn blood vessels to prevent apoptotic response and cellular death [16]. Also, cancer cells block the apoptosis response by suppressing the cell apoptotic gene expression profile such as Caspase 3 and BAX genes [17, 18]. Therefore, investigating the selective apoptotic and anti-angiogenic bioactive compounds has the potential to efficiently suppress carcinogenesis without undesired harmful side effects.

The current non-specific cancer therapy strategies for lung and colon cancers have not efficiently suppressed their angiogenesis process and migration rate. In this regard, the targeted cancer therapy strategies have been applied by utilizing the novel transporting carriers of the anti-oxidant, anti-angiogenic, and anticancer bioactive compounds called nano-drug delivery systems (NDDS). The NDDS is made of bio-compatible nanostructured polymeric and/or amphipathic compounds, which improve their cargo's chemical activity in *In-Vivo* conditions [19, 20]. In other words, designing the nanostructured molecular cages as drug encapsulating systems facilitates the release, delivery, and cellular uptake processes regulation. Among various types of NDDS' structural components, polycationic polymers such as chitosan have widely been used as the most biocompatible encapsulating molecule in several types of NDDS [20–23].

There are several types of synthetic chemical anticancer compounds have been used for suppressing the human lung and colon carcinogenesis processes such as bleomycin, doxorubicin, etoposide (VP-16), cisplatin, methotrexate, Irinotecan, 5-fluorouracil, and Oxaliplatin. However, the high-risk undesired harmful side effects are still their main limitations as an anticancer compound [24, 25]. Therefore, the researchers have focused on the natural and safe phytochemical-based anticancer compounds as the next efficient chemotherapy substituents such as crocin, curcumin, hesperidin, and urolithins [26–30].

Urolithins are dibenzopyran derivatives produced by human gut microbiota after consuming ellagitannins (ET)-containing foods, such as nuts, pomegranates, and berries. They exhibit anticancer impacts by inducing cell cycle arrest, apoptosis response, and suppressing angiogenesis. Methyl urolithin-A is a derivative of urolithin A, which has shown anti-cancer and antioxidant properties [31, 32]. The aim of this study is to develop and evaluate the properties of Methyl urolithin A-loaded folate-chitosan nanoparticles (Mu-PFCNPs) for their potential antioxidant, anti-angiogenic, and selective anticancer activities against human colorectal (HT-29), ovarian (A2780), pancreatic (PANC), and liver (HepG2) cancer cell lines. This research focuses on utilizing Mu-PFCNPs as a promising therapeutic approach for cancer treatment based on the known anti-cancer and antioxidant properties of methyl urolithin A. However, the study only investigates the potential effects of Mu-PFCNPs on four specific cancer cell lines (HT-29, A2780, PANC, and HepG2). While these cell lines represent various types of cancer, the research may not cover the entire spectrum of cancer types, which could limit the generalizability of the findings. Moreover, the study is conducted in a controlled laboratory setting using cell cultures, which are in vitro experiments. While these experiments provide valuable insights into the potential effects of Mu-PFCNPs on cancer cells, further *in vivo* studies (using animal models) and clinical trials are necessary to confirm the safety and efficacy of Mu-PFCNPs in real-world conditions and to establish their potential as a therapeutic treatment for cancer patients.

Materials and methods

Materials

Methylurolithin-A (MuA)(Golexir, Iran), Folic acid, Polymeric nanospheres of poly (lactic-co-glycolic) acid (PLGA) (50-50)(Sigma Aldrich, France), Polyvinyl alcohol PVA ethyl(dimethylaminopropyl)carbodiimide / N-hydroxysuccinimide (EDC/NHS)(Merck, Germany), Chitosan (LMW), 2,4,6-tripyridyl-s-triazine (TPTZ), 2,2-Diphenyl-1-picrylhydrazylradical (DPPH), 2,2′-azinobis (3-ethylbenzothiazoline-6-sulfonic acid) (ABTS), 3-(4,5-dimethylthiazol-2-yl)-2,5-diphenyltetrazolium bromide (MTT), and dimethylsulfoxide (DMSO) were purchased from Merck company. The human lung cancer A2780, HT-29, PANC, and HepG2 cell lines were provided by the Pastore Institute of Iran.

Mu-PFCNPs Synthesis

The Mu-PFCNP synthesis was conducted in two steps, producing Methylurolithin-A-loaded PLGA nanoparticles (Mu-PNPs) and coating them with a thin folate-linked chitosan layer. PLGA which is approved by the Food and Drug Administration (FDA), is known to be safe for medical applications due to its bioavailability and biodegradable profile. One of the advantages of PLGA nanoparticles is that they trap highly volatile compounds and their production can be carried out at room temperature. To produce Mu-PNPs, an organic phase consisting of dissolved PLGA in DMSO solvent was prepared. Then, MuA (1 mg/mL) and PVA (2% W/V) solutions were added to the prepared organic phase at the optimal proportions. The final biphasic mixture was homogenized by applying a probe sonicator at 350 W power for 10 minutes (8" On 2" Off). The homogenized mixture was exposed to PVA (1% W/V) solution under continuous stirring conditions for 2 hours. The produced Mu-PNPs were extracted and purified by centrifuging at 12000 rpm for 5 minutes. The pellet was lyophilized utilizing a -80°C-freeze drier device [33].

The second step was conducted by coating the MuA-PNPs with the folate-linked chitosan layer. The folic acid was dissolved in DMSO and its carboxylic acid functional groups were activated by EDC (10 mM) exposure. On the other hand, the acetic acid (2% V/V) chitosan solution (1% W/V) was provided and exposed to NHS (5 mM) solution to activate the chitosan amin functional groups. The activated folate and chitosan solutions were mixed and stirred for an overnight incubation period to produce a folate-linked chitosan (FC) polymer. The FC precipitate was rinsed with deionized water and lyophilized. Finally, the Mu-PNPs mixture and FC solution (1% V/V acetic acid solvent) were gradually mixed and incubated for a further 2 hours under continuous stirring conditions [34, 35].

Mu-PFCNPS characterization

To determine the average hydrodynamic size of the Mu-PFCNPs, dynamic light scattering (DLS) analysis was utilized by applying (Zetasizer (nanoparticle SZ-100)). The Mu-PFCNP chemical properties were studied by recording the MuA, chitosan, folic acid, and PLGA wave numbers utilizing FTIR spectroscopy (4000 to 400 cm^{-1} wavenumbers at 4 cm^{-1} resolution. Finally, the nanoparticles' stability was evaluated by measuring their surface charge (Zetasizer (nanoparticle SZ-100). Finally, the nanoparticles' shape and dehydrated size were studied by applying Field emission scanning electron microscopy (FESEM). To this purpose, 50 µL of the Mu-PFCNPs mixture was dried on the aluminum foil to be coated with gold ions before initiating the imaging process of microscopy.

MuA loading and releasing efficiency

The MuA loading efficiency into the PLGA nanocarriers was estimated by calculating the MuA concentration before and after MuA-PNP formation. The MuA concentration was measured by providing the standard absorbance diagram at 217 nm absorbance (visible-ultraviolet spectrophotometer (Hutch, USA).

Mu-PFCNPS antioxidant activity

ABTS assay

The Mu-PFCNPs antioxidant activity was evaluated measuring their radical scavenging potential. To this purpose, potassium persulfate (2.45 mM) was provided to activate the ABTS· radicals. The activated ABTS was incubated at 25°C in dark conditions for 14 hours. Then, 5 µL of different concentrations of Mu-PFCNPs mixture (62.5, 120, 250, 500, 1000, and 2000 µg/mL) was added to the activated ABTS solution (3.995 mL). The samples' absorbance was measured at 743 nm after 30 minutes of incubation in dark conditions [36, 37]. The Mu-PFCNPs antioxidant activity was expressed as the ABTS inhibition rate (AIR%) calculated by the following equation:

$$AIR\% = A\ control - A\ sample/A\ control \times 100$$

DPPH assay

To measure the Mu-PFCNPs antioxidant activity, the DPPH radical inhibition rate was analyzed by recording the DPPH absorbance at 517 nm following 30-min

incubation of ethanolic DPPH (0.05 mg/mL) with a range of Mu-PFCNPs concentrations (62.5, 120, 250, 500, 1000, and 2000 µg/mL) in dark conditions [37]. The DPPH inhibition rate (DIR%) was calculated as the following equation:

$$DIR\% = A\ control - A\ sample / A\ control \times 100$$

FRAP assay

The Fe^{+3}- reductive potential of Mu-PFCNPs was evaluated by applying FRAP assay. Briefly, equal volumes of TPTZ (10 mM), $FeCl_3$ (20 mM), and acetate buffer (300 mM) were mixed to provide the FRAP reagent solution. The Iron-reductive potential of Mu-PFCNPs was measured by adding FRAP reagent (280 µL) to 20 µL of different concentrations of the nanoparticles (0.2, 0.4, 0.8, 1.2, 1.6, and 2 mg/mL) and kept in dark conditions for 5 minutes., The product absorbance was recorded at 539 nm as the reduced Fe^{+2} concentration, which was calculable by the $FeSO_4$ standard diagram [38].

MTT assay

All cancer (PANC, A549, A2780, HepG2, and HT-29) and normal Huvec cell lines were seeded at cell density of 4×10^3 cells/cm^2 and cultured in cell culture medium (DMEM) supplemented with FBS (10% V/V) and streptomycin/penicillin (100 mg/mL:100U/mL) at standard conditions (95% humidity, 5% CO2, 37 °C) for a 24-hour incubation period. The cells were harvested and cultured in 96-well plates (4×10^3 cells/well) for 24 hours. Then, the cells were treated with different concentrations of the Mu-PFCNPs (31.2, 62.5, 125, 250, and 500 µg/mL) and incubated for 48 hours. Next, the media was refreshed with fresh MTT (0.5 mg/mL)-supplemented media and kept for a further 3 hours at 37°C. Finally, the media was drained and the produced formazan was dissolved in DMSO solvent to record its absorbance at 570 nm (Stat fax 2100 plate reader). The formazan concentration was considered as the cells' survival indicator and calculated using the following equation [39]:

$$Cell\ survival\ (\%) = (sample\ absorbance\ /\ control\ absorbance) \times 100$$

CAM assay

The Mu-PFCNP's angiogenic property was studied by conducting a CAM assay. Briefly, 40- disinfected fertilized eggs were provided and incubated in the incubator for 48 hours at standard conditions (60% humidity, 37°C). Then, a $1cm^2$ window was cut at their eggshell and sealed with paraffin under sterile conditions. The eggs passed a 6-day incubation period at the same conditions with twice rotation per day. Then, the treatment process was conducted utilizing small gelatin sponge sections smeared with different doses of Mu-PFCNPs, which were made by applying agar, egg whites, and antibiotics. The smeared sponges were placed on the chorioallantoic membrane just before the resealing process. After a further 72-hour incubation period, the eggs' chorioallantoic membrane and the formed embryos were studied by taking several images, which were finally analyzed by applying Image J software to analyze the embryos' weight/length and the length/number of the CAM blood vessels [40].

Gene expression profile

The angiogenic (*VEGF* and *VEGFR*) and antioxidant (*SOD* and *CAT*) gene expression profiles were provided on the human colon HT-29 cancer cells. Briefly, the total RNA contents of the 48-hour exposed incubated cells were extracted by applying an RNA extraction kit (Pars tous, Iran). Then, their related cDNA libraries were synthesized utilizing a cDNA synthesis kit (Pars tous, Iran). The target gene primer sets were designed at the exon junction sites of the VEGF *VEGFR, SOD,* and *CAT* genes by Allel ID6 software (Table 1). The targeted cDNAs were detected by conducting PCR technique (Bio-Rad CFX96). To genes' fold changes were estimated utilizing the Q-PCR method using a SYBER green-containing PCR master mix (Qiagen, Hilden, Germany) and normalized by measuring the *GAPDH* control gene expression.

Table 1 The PCR primer sets of target genes (VEGF and VEGFR)

Gene	Forward sequence	Reverse sequence
GAPDH	GCAGGGGGGAGCCAAAAGGGT	TGGGTGCCAGTGATGGCATGG
VEGF	CCTCCGAAACCATGAACTTT	TTCTTTGGTCTGCATTCACATT
VEGFR	CCAGTCAGAGACCCACGTTT	AGTCTTTGCCATCCTGCTGA
SOD	CAGCATGGGTTCCACGTCCA	CACATTGGCCACACCGTCCT
CAT	CGTGCTGAATGAGGAACAGA	AGTCAGGGTGGACCTCAGTG

Statistical analysis

One-way ANOVA test (SPSS-20 software) was used for providing the data significance levels at less than 0.001, 0.01, and 0.05 P-values, which were considered as the statistically significance levels indicated as ***, **, and * indices.

Results

Mu-PFCNPS characterization

The hydrodynamic size of Mu-PFCNPs was measured at 314.4 nm (Fig. 1A). To verify the measured size reliability, the Poly-dispersed Index (PDI) of the nanoparticles was estimated. The reported nanoparticles' PDI index of 0.332 indicated the monodispersed formation process [41], which verifies the estimated size accuracy. Moreover, the Mu-PFCNPs formation process was studied by analyzing their chemical structural bonds and functional groups of their components including MuA, PLGA, folic acid, and chitosan, which was provided by FTIR spectroscopy shown in Fig. 1B. Considering the results, the appeared bonds at the vibrational 3400–3200 cm^{-1} wavenumbers refer to the phenolic hydroxyl group (stretching vibrations of O–H bonds) of MuA [42]. Also, the bond appeared at 1658.38 cm^{-1} referring to the stretching –COO bonds of PLGA. The folate structure was detected by observing 1437.25 cm^{-1} (CH–NH-C=O amides cm^{-1}); and 901.25 cm^{-1} (the benzene aromatic C–H bending vibrations) [43]. Finally, Chitosan was detected by observing the appeared bond at 2914.33 and 2999.31 cm^{-1}, which introduce the symmetric and asymmetric C-H stretching vibrations, respectively [44]. The Folate-Chitosan coating layer not only improves the Mu-PFCNPs selective delivery but also makes Mu-PFCNPs surface charge positive (+30.14 mV), which enables them

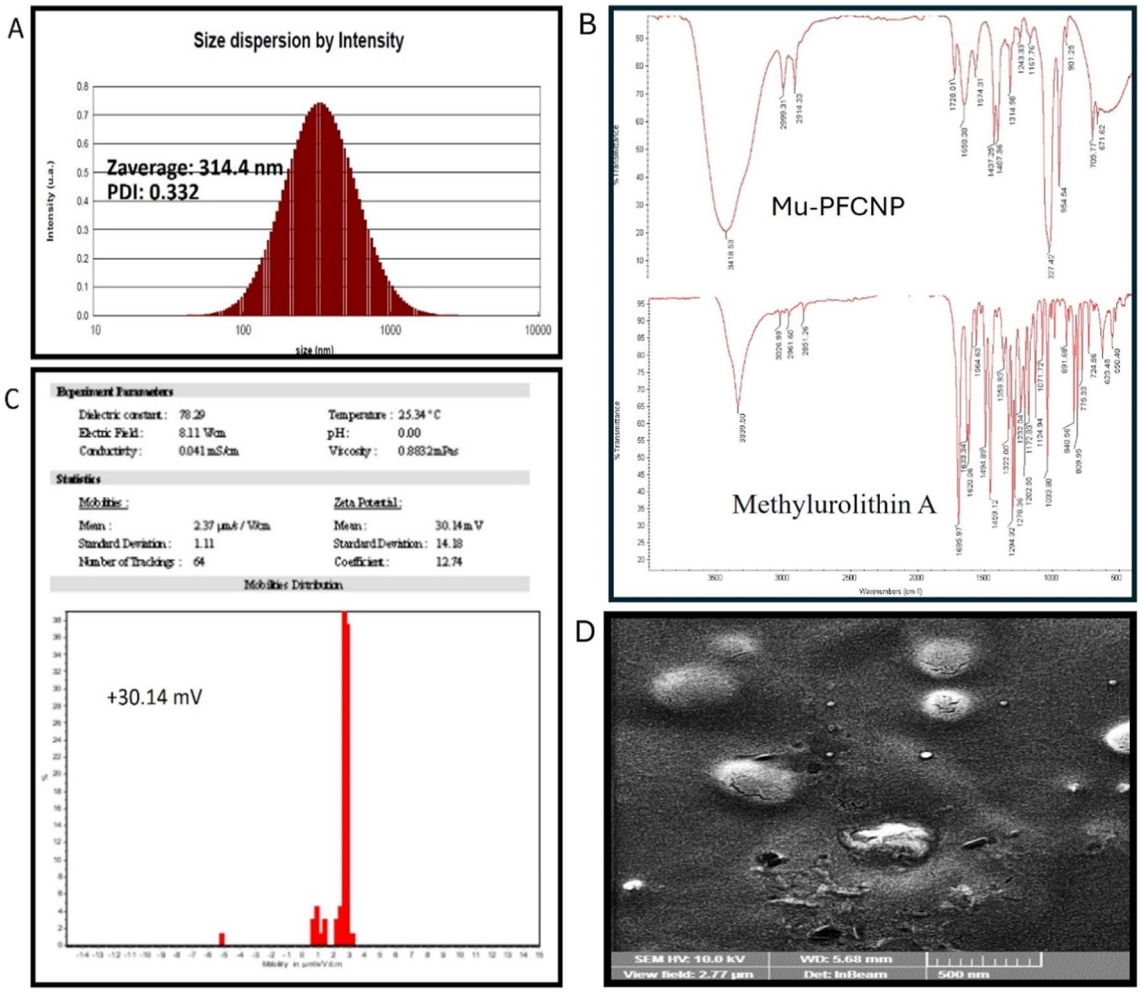

Fig. 1 The Mu-PFCNPs size characterization. (**A**) The nanoparticles' DLS-reported size distribution. (**B**) and (**C**) indicate the FTIR pattern and surface zeta potential of the nanoparticles, respectively. (**D**) The FESEM micrograph of the dehydrated Mu-PFCNP size and morphology. Mu-PFCNPs: Methylurolithin A-loaded folate-chitosan nanoparticles

to easily pass the cell membrane and not be aggregated in an aqueous solution (Fig. 1C) [45]. Finally, the spherical 134-nm nanoparticles dehydrated Mu-PFCNPs' were reported by the FESEM microscopy analysis (Fig. 1D).

MuA loading efficiency

The MuA loading efficiency was estimated according to the MuA standard concentration in physiologic pH (7.4). The result exhibited the 77.9 % entrapment rate of MuA into the produced nanoparticles, Fig. 2

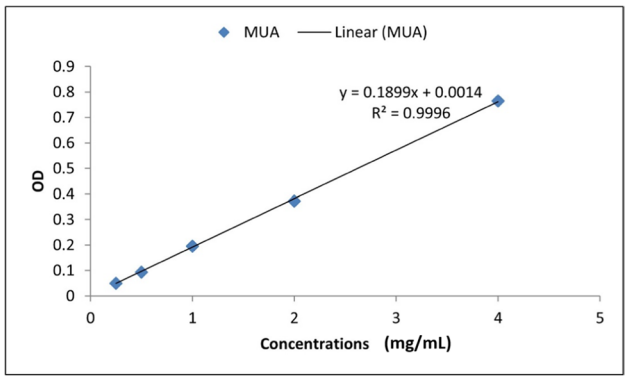

Fig. 2 The Methylurolithin-A loading efficiency. Mu-PFCNPs: MuA-loaded PLGA-folate-chitosan nanoparticles.

The Mu-PFCNPS antioxidant activity

A significant radical scavenging activity was detected following the increased Mu-PFCNP doses. In other words, the weak antioxidant potential of the Mu-PFCNPs at less than their non-toxic doses for all the cancer cell lines in both cancer and normal cells shows their promotive potential in inducing the cancer cell death process by indirect ROS accumulation near the cancer cells (Fig. 3).

The Mu-PFCNPs' influence on the antioxidant defense system enzymes, such as SOD and CAT, primarily resulted in a significant down-regulation of SOD (as depicted in Fig. 4). The substantial increase in SOD gene expression due to the elevated Mu-PFCNPs exposure reveals the nanoparticles' pro-oxidant activity, which acts synergistically with their cytotoxic activity. This pro-oxidant effect can be interpreted as an advantageous factor in enhancing the anticancer potential of the treatment. Furthermore, the primary down-regulation of SOD might be effective in increasing the dismutation of superoxide radicals, which in turn improves the anticancer potential [46]. The lack of significant impact of Mu-PFCNPs on the CAT gene expression suggests that the nanoparticles have a null effect on the CAT-mediated antioxidant response following the cell treatment process. This characteristic could be beneficial for normal cells expressing the CAT-mediated antioxidant defense pathway, as it would not be affected by the Mu-PFCNPs treatment.

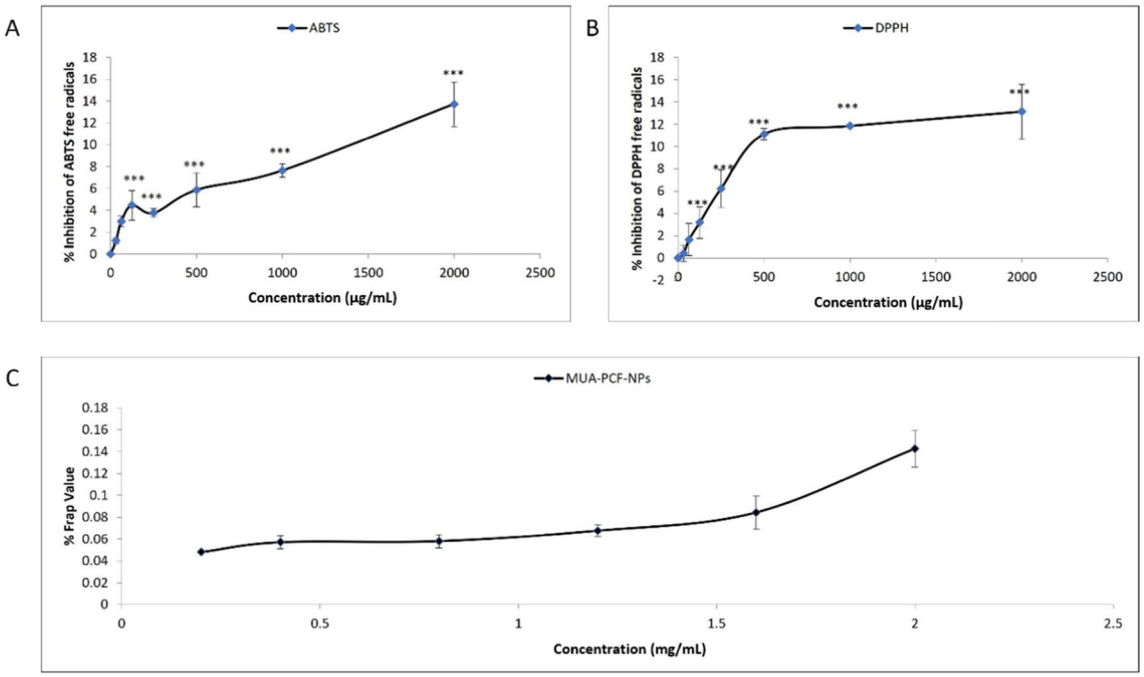

Fig. 3 The Mu-PFCNP activity in scavenging the ABTS, DPPH and FRAP free radicals. The *** indicates the p-Value < 0.001. The error bars represent the standard error of the mean (SEM). Mu-PFCNPs: MuA-loaded PLGA-folate-chitosan nanoparticles

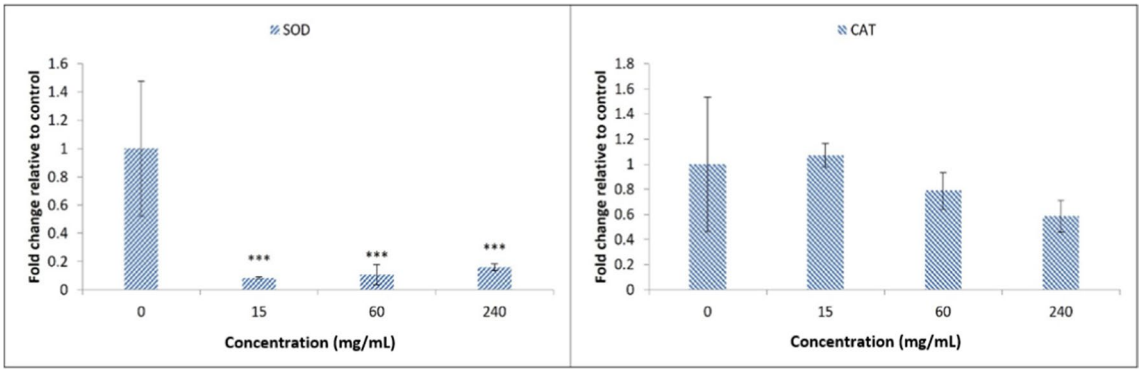

Fig. 4 The antioxidant defense enzyme gene expression profile of the HT-29 cancer cell line following the Mu-PFCNPs exposure. The *** indicate the p-Values < 0.001. The error bars represent the standard error of the mean (SEM). Mu-PFCNPs: MuA-loaded PLGA-folate-chitosan nanoparticles

Additionally, a recent study has demonstrated that the pro-oxidant activity of nanoparticles can enhance the production of reactive oxygen species (ROS) in cancer cells, leading to increased cellular damage and ultimately, cell death [47]. This further supports the synergistic effect of Mu-PFCNPs' pro-oxidant and cytotoxic activities in promoting anticancer potential.

The Mu-PFCNPS cytotoxicity

The significant cell-selective cytotoxic impact of the Mu-PFCNPs nanoparticles is evident from the results presented in Fig. 5. The maximum and minimum values of the IC_{50} index of the Mu-PFCNPs were established in the HepG2 and HT-29 cancer cell lines, respectively. The normal Huvec and cancerous PANC cell lines were the only cells that completely survived the treatment process. Furthermore, the most sensitive cancer cells to the Mu-PFCNPs were the HT-29 (IC50=60 µg/mL), A549 (IC50=150 µg/mL), A2780 (IC50=204 µg/mL), and HepG2 (IC50=500µg/mL, respectively. The IC_{50} index of the Mu-PFCNPs in HT-29 cancer cells was significantly lower than their values in Huvec, PANC, and other cancer cell lines. This suggests that the Mu-PFCNPs have the potential to selectively target and deliver to the HT-29 cancer cells. This selective targeting can be attributed to the overexpression of folate receptors in the HT-29 cancer cells. It has been reported that folate receptor overexpression is a common characteristic in several types of cancer, including ovarian, colon, and endometrial cancers, which can be exploited for targeted drug delivery [48]. Therefore, the Mu-PFCNPs' selective targeting of HT-29 cancer cells can be attributed to the overexpressed folate receptors on their surface, making them an effective tool for targeted cancer therapy.

The Mu-PFCNPS anti-angiogenic activity

Upon exposure of HT-29 cells to varying concentrations of Mu-PFCNPs, a substantial alteration in the *VEGF* and *VEGFR* gene expression profiles was observed (Fig. 6). To further elucidate this phenomenon, two additional scientific supporting paragraphs have been added. The results indicated that low doses of Mu-PFCNPs led to a significant decrease in both *VEGF* and *VEGFR* gene expression levels. This down-regulation suggests that the initial interaction between HT-29 cells and Mu-PFCNPs may inhibit angiogenesis, a crucial process in tumor growth and metastasis. Secondly, to understand the response of HT-29 cells to high-dose Mu-PFCNP treatment, a detailed investigation was performed. The findings revealed that the up-regulation of *VEGF* in this case could be attributed to the activation of a cancer cell anti-dote resistance mechanism. This response allows the cells to counteract the effects of the Mu-PFCNPs, thereby maintaining their proliferative capabilities and promoting tumor growth. In conclusion, the exposure of HT-29 cells to Mu-PFCNPs resulted in significant changes in *VEGF* and *VEGFR* gene expression levels. Low doses of Mu-PFCNPs inhibited angiogenesis by down-regulating these genes, while high-dose treatment triggered a resistance mechanism, up-regulating *VEGF* and promoting cancer cell survival. The *VEGF* and *VEGFR* down-regulation has the potential to efficiently inhibit angiogenesis by suppressing the *VEGF* secretion and preventing its receptor-expressing, respectively.

As shown in Fig. 6 the CAMs exposed to the increased Mu-PFCNP concentrations exhibited a meaningful decrease in the count and length of the CAM blood vessels, which revealed the Mu-PFCNP's suppressive impact on the angiogenesis process (P-value < 0.001). Moreover, a negative significant correlation was measured between the embryos' growth inhibition rate and the increased

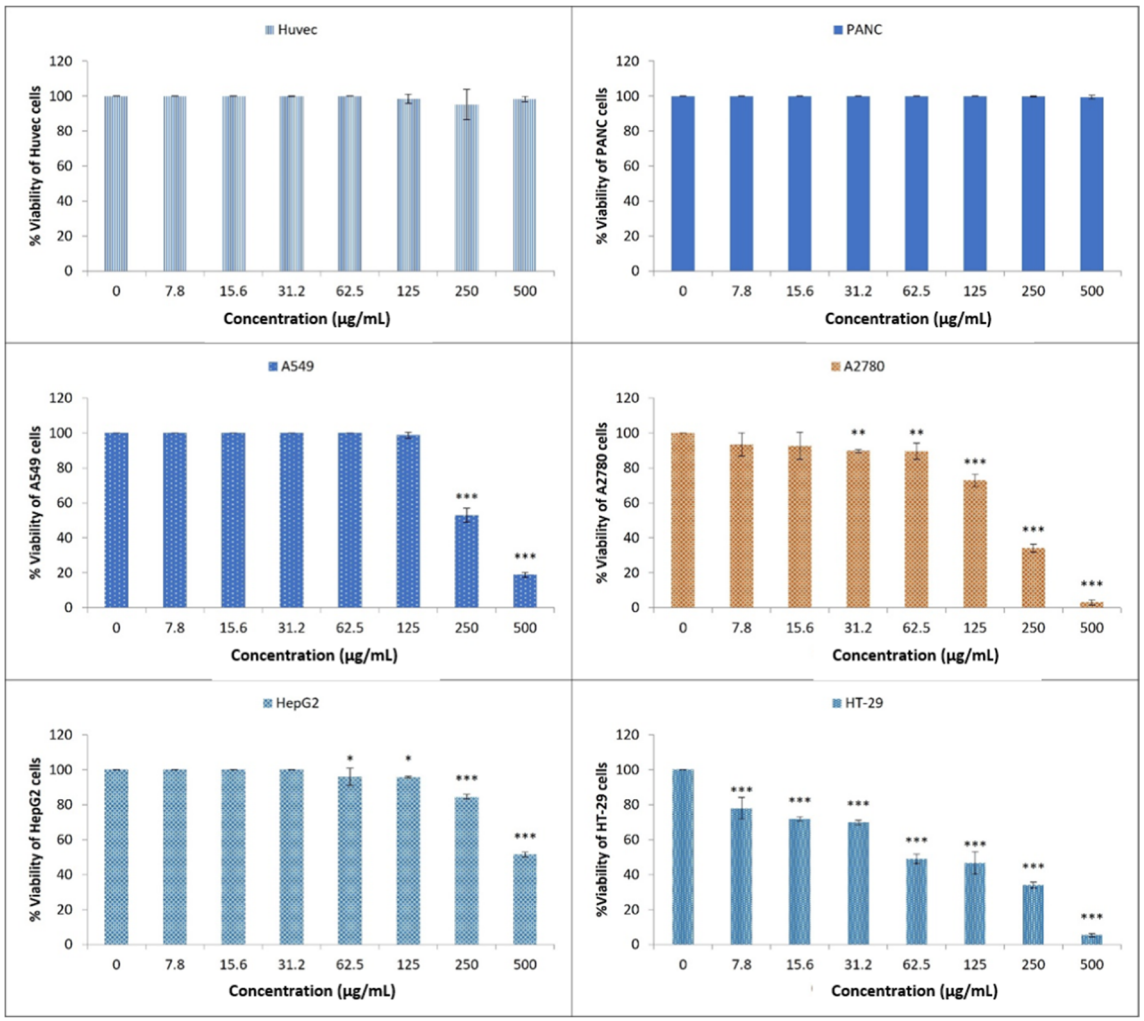

Fig. 5 The 48-hour treated cell survival in response to the increased Mu-PFCNPs treatment doses. The *, **, and *** indicate the p-Values < 0.05, < 0.01, and < 0.001, respectively. The error bars represent the standard error of the mean (SEM). Mu-PFCNPs: MuA-loaded folate-chitosan nanoparticles

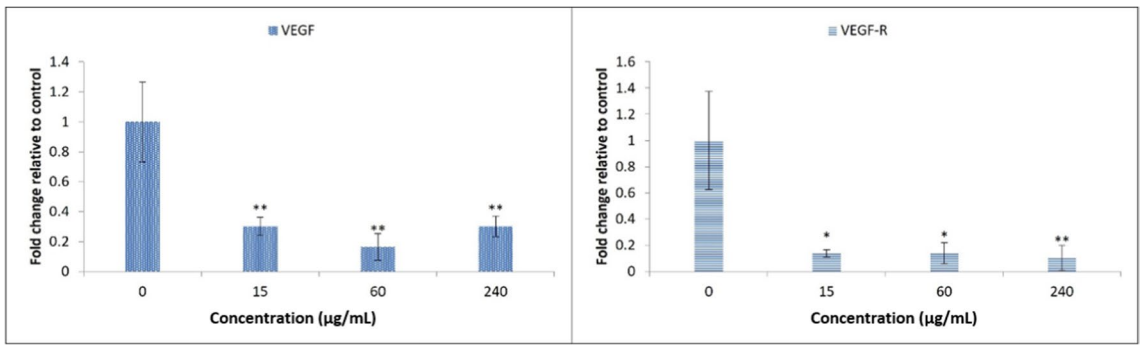

Fig. 6 The *VEGF* and *VEGFR* gene expression alteration following the increased Mu-PFCNP treatment concentration in the CAM tissue. The * and ** indicate the p-Values < 0.05 and < 0.01 respectively. The error bars represent the standard error of the mean (SEM). Mu-PFCNPs: MuA-loaded PLGA-folate-chitosan nanoparticles

Mu-PFCNPs treatment concentrations (P-value < 0.001) (Fig. 7A and B).

Down-regulating the *VEGF* and *VEGFR* has the potential to completely suppress the angiogenesis process by blocking both the angiogenesis stimulator and its receptor-mediated cellular uptake in the treated cancer cells.

Discussion

The grim outlook for human colon cancer, its delayed detection, escalating mortality rates, and inadequate treatment efficacy pose significant challenges that necessitate the development of innovative therapeutic approaches. Consequently, research has focused on natural selective anticancer bioactive compounds as potential treatment options. To address the aforementioned issues, a variety of chitosan/PLGA-based organo-tropic nano-transporters have been meticulously designed, manufactured, and proposed as selective nano-drug delivery systems for combating various types of human cancers. Furthermore, scientific studies have demonstrated the effectiveness of these chitosan/PLGA-based nano-transporters in enhancing drug delivery and improving treatment outcomes. For instance, it has been reported that these nano-transporters significantly increased the bioavailability and targeted delivery of anticancer drugs, leading to improved therapeutic efficacy and reduced side effects. The potential of these novel nano-drug delivery systems in overcoming the challenges associated with human colon cancer treatment. [49–51]. In the current study, MuA was encapsulated into the chitosan-coated PLGA nanoparticles decorated with folic acid ligands to improve the MuA bio-accessibility and functionalize its delivery to the folate receptor-positive cancer cells. The Mu-PFCNPs were successfully produced, characterized, and analyzed in case of their antioxidant, anti-angiogenic, and selective cytotoxicity. The results exhibited a significant antioxidant, anti-angiogenic, and selective HT-29 cytotoxicity of the Mu-PFCNPs.

Cancer cell survival relies on the activation of intricate biochemical pathways that supply the necessary metabolic

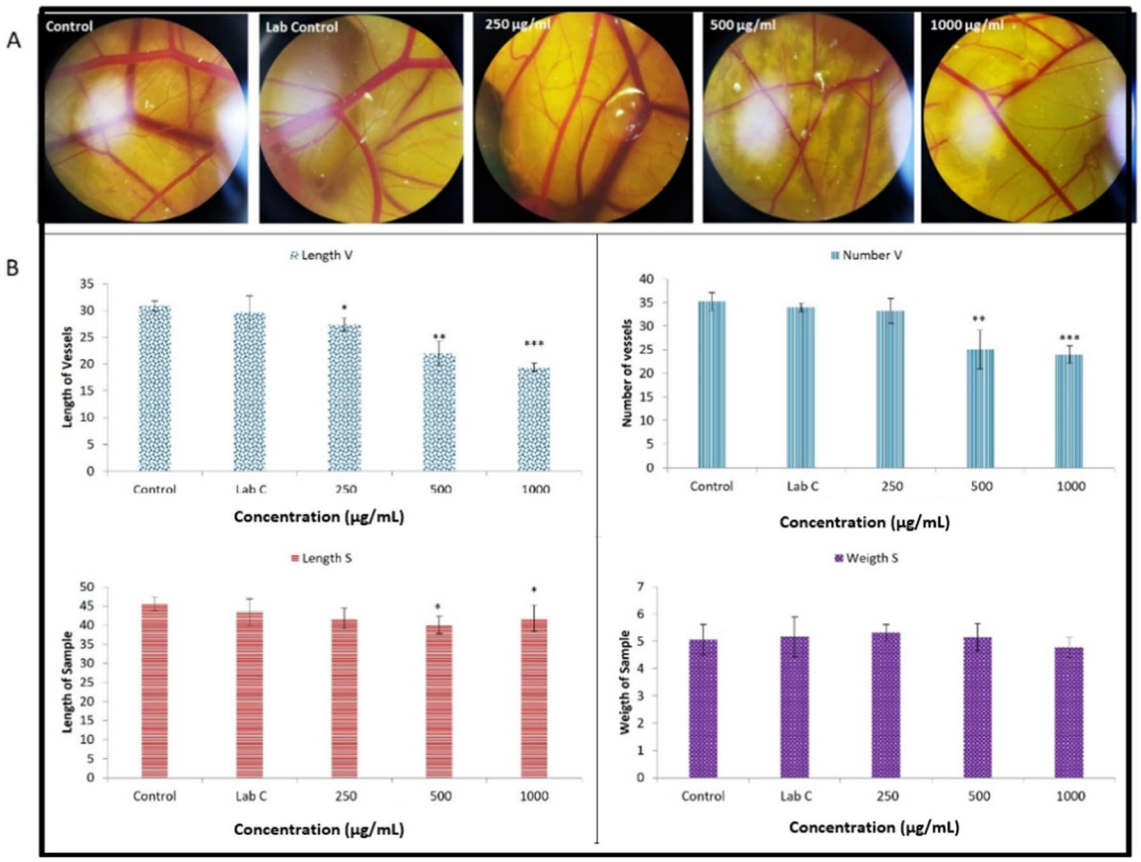

Fig. 7 The Mu-PFCNPs antiangiogenesis activity. (**A**): Refers to the significant dose-dependent decreasing impact of different doses of Mu-PFCNPs (250, 500, and 1000 µg/mL) on the numbers of chorioallantoic blood vessels compared with control (not treated) and Lab control (normal saline treatment). (**B**): Refers to the chorioallantoic blood vessels length and number, and embryos' length and weight in response to different doses of Mu-PFCNPs. The *, **, and *** indicate the p-Values < 0.05, < 0.01, and < 0.001, respectively. The error bars represent the standard error of the mean (SEM).Mu-PFCNPs: MuA-loaded PLGA-folate-chitosan nanoparticles

bioenergetics, such as folic acid, to support their growth. Additionally, these cells possess a robust antioxidant defense system, which includes enzymes like superoxide dismutase (*SOD*) and catalase (*CAT*), to combat the reactive oxygen species generated during cellular metabolism. Moreover, cancer cells exhibit aggressive angiogenesis, facilitated by the up-regulation of vascular endothelial growth factor (*VEGF*) and its receptor (*VEGFR*), allowing them to form new blood vessels for migration and nutrient supply. This complex interplay of biochemical processes highlights the importance of understanding cancer cell biology to develop effective therapeutic strategies [52–55]. Therefore, targeting the cancer folate receptor can be applicable for selective drug delivery. Moreover, investigating therapeutics suppressing the cancer cell antioxidant defense system (*SOD* and *CAT* down-regulation) and angiogenesis ability makes the cells vulnerable to drug-induced oxidative stresses and suppresses their migration.

MuA, the main human gut microbiota byproduct has been reported as a natural potent antioxidant and anticancer compound [31, 32]. However, its short-time chemical activity and weak solubility in *in-vivo* conditions have limited their bioactive efficiency.

Introducing the nanodrug delivery systems has opened a promising way of overcoming drug delivery limitations. Their chemical structure enables them to be desired nanocarriers compatible with their cargo's chemical properties and environmental conditions in case of polarity, acidity, and temperature details.

In the recent study, the researchers have explored the potential of PLGA and chitosan polymers as the primary and secondary protective barriers for the MuA molecule. The weak radical scavenging activity observed in the Mu-PFCNPs can be attributed to the efficient gradual release of MuA, which showcases its synergistic anticancer co-stimulating potential. In simpler terms, the Mu-PFCNPs demonstrated weak significant antioxidant activity, functioning as a shield for normal cells from oxidative stress while accumulating oxidants in cancer cells below their toxic IC_{50} concentrations in HT-29 cancer cells. The synergistic interaction between the MuA molecule and the protective polymers can be the enhanced antioxidant capacity of the Mu-PFCNPs. This additional information highlights the importance of the polymers in the overall performance of the Mu-PFCNPs and their potential in cancer therapy.

To enhance the folic acid decoration on nanocarriers, chitosan, which possesses multiple amine functional groups, has been chosen. The primary mechanism behind this selection involves the interaction between the main-carboxyl group of chitosan and the iso-peptide bond formation with folic acid elements. This interaction leads to the successful functionalization of Mu-PFCNPs, a crucial aspect contributing to their selective cytotoxicity. As reported in a scientific study [56], this functionalization not only improves the stability and aqueous solubility of Mu-PFCNPs but also showcases remarkable selective cytotoxicity towards the human colon HT-29 cell line when compared to other normal and cancerous cells. This highlights the effectiveness of chitosan in facilitating the desired properties in Mu-PFCNPs for targeted drug delivery applications.

It can be inferred that the variation in IC_{50} concentrations of Mu-PFCNPs between exposed normal and cancerous cells signifies the receptor-mediated endocytosis mechanism for the cellular uptake of Mu-PFCNPs. As per the proposed hypothesis, the cellular uptake is directly influenced by the frequency of folate receptors present on the treated cells. Consequently, cells with a higher density of folate receptors exhibit increased nanocarrier uptake, leading to rapid suppression compared to those with fewer receptors. This observation aligns with scientific studies demonstrating the targeting efficiency of folate-conjugated nanoparticles in cancer therapy, where cancer cells typically overexpress folate receptors, enabling selective and efficient drug delivery [57].

Conclusion

The MuA novel formulated nano drug delivery system not only decreases the SOD antioxidant gene expression of the treated HT-29 cancer cells but also has the potential to protect normal cells at its IC_{50} concentration in HT-29 cells, which indicates its dual cell protective and cytotoxic role for normal and cancerous cells, respectively. Moreover, the anti-angiogenic and cell-selective toxicity of the Mu-PFCNPs makes them a powerful multifunctional anti-colon cancer compound. However, there are several pharmaceutical parameters have to be studied to clarify their treatment efficiency in *in-vivo* conditions.

Acknowledgment This work was supported by, Islamic Azad University, Mashhad, Iran, and therefore is appreciated by the author.

Author contributions All authors contributed to the study conception and design. Material preparation, data collection were performed by [AJZA] and [VP]. Supervised and analysis were performed by [VP] and [MHT]. The first draft of the manuscript was written by [VP] and [AJZA], all authors commented on previous versions of the manuscript. All authors read and approved the final manuscript.

Funding No funding was received for conducting this study.

Data availability The datasets used and analyzed during the current study are available from the corresponding author on reasonable request.

Declarations

Competing interests The authors declare no competing interests.

Ethics Approval Not applicable.

Consent for Publication All authors are happy with this publication.

Competing interest The authors declare no competing interests.

References

1. J. M. Peters and F. J. Gonzalez (2018). The evolution of carcinogenesis. *Toxicological sciences* **165** (2), 272–276.
2. S. I. Hashemy and S. M. R. Seyedi, ROS impacts on cell cycle checkpoint signaling in carcinogenesis,. Handbook of oxidative stress in cancer: mechanistic aspects. Springer, pp 1–19.
3. H. Sung, et al. (2021). Global cancer statistics 2020: GLOBOCAN estimates of incidence and mortality worldwide for 36 cancers in 185 countries. *CA: A Cancer Journal for Clinicians* **71** (3), 209–249.
4. J.-X. Hu, et al. (2021). Pancreatic cancer: A review of epidemiology, trend, and risk factors. *World journal of gastroenterology* **27** (27), 4298.
5. H. Rumgay, et al. (2022). Global burden of primary liver cancer in 2020 and predictions to 2040. *Journal of Hepatology* **77** (6), 1598–1606.
6. A. Mazidimoradi, et al. (2022). The global, regional and national epidemiology, incidence, mortality, and burden of ovarian cancer. *Health Science Reports* **5** (6), e936.
7. F. Perlikos, K. J. Harrington, and K. N. Syrigos (2013). Key molecular mechanisms in lung cancer invasion and metastasis: a comprehensive review. *Critical reviews in oncology/hematology* **87** (1), 1–11.
8. S. Hazell, et al. (2020). Financial toxicity in lung cancer: an assessment of magnitude, perception, and impact on quality of life. *Annals of Oncology* **31** (1), 96–102.
9. Y. Liu, et al. (2023). Formation of pre-metastatic niches induced by tumor extracellular vesicles in lung metastasis. *Pharmacological Research* **188**, 106669.
10. N. Vaquero-Siguero, et al. (2022). Modeling colorectal cancer progression reveals niche-dependent clonal selection. *Cancers* **14** (17), 4260.
11. R. V. Cardoso, et al. (2022). Trends in drug delivery systems for natural bioactive molecules to treat health disorders: the importance of nano-liposomes. *Pharmaceutics* **14** (12), 2808.
12. C.-I. Chen, et al. (2022). High expression of folate receptor alpha (FOLR1) is associated with aggressive tumor behavior, poor response to chemoradiotherapy, and worse survival in rectal cancer. *Technology in Cancer Research & Treatment* **21**, 15330338221141796.
13. M. J. Birrer, et al. (2019). Is targeting the folate receptor in ovarian cancer coming of age? *The Oncologist* **24** (4), 425–429.
14. I. Vergote and C. P. Leamon (2015). Vintafolide: a novel targeted therapy for the treatment of folate receptor expressing tumors. *Therapeutic advances in medical oncology* **7** (4), 206–218.
15. Y.-Y. Wang, et al. (2022). Development of a novel multi-functional integrated bioconjugate effectively targeting K-Ras mutant pancreatic cancer. *Journal of Pharmaceutical Analysis* **12** (2), 232–242.
16. M. Ushio-Fukai and Y. Nakamura (2008). Reactive oxygen species and angiogenesis: NADPH oxidase as target for cancer therapy. *Cancer letters* **266** (1), 37–52.
17. Güneş Bayır A., ROS in Apoptosis of Cancer Cells, -Handbook of Oxidative Stress in Cancer: Mechanistic Aspects-, Sajal Chakraborti,Bimal K Ray, SushantaRoychowdhury, Editör, Springer, London/Berlin, Singapore, ss.1-13, 2021
18. Z. Liu, et al. (2016). Direct activation of Bax protein for cancer therapy. *Medicinal research reviews* **36** (2), 313–341.
19. V. V. Veselov, et al. (2022). Targeted delivery methods for anticancer drugs. *Cancers* **14** (3), 622.
20. V. P. Chavda, et al. (2022). Nano-drug delivery systems entrapping natural bioactive compounds for cancer: recent progress and future challenges. *Frontiers in oncology* **12**, 867655.
21 Y. Herdiana, et al. (2022). Drug release study of the chitosan-based nanoparticles. *Heliyon* **8**, e08674.
22. Al-Hasnawi HNG, Pouresmaeil V, Davoodi-Dehaghani F, Rahban S, Pouresmaeil A, Homayouni Tabrizi M. Synthesis Folate-linked Chitosan-coated Quetiapine/BSA Nano-Carriers as the Efficient Targeted Anti-Cancer Drug Delivery System. Mol Biotechnol. 2023 Aug 26. https://doi.org/10.1007/s12033-023-00858-0
23. Alkwedhim MAH, Pouresmaeil V, Davoodi-Dehaghani F, Mahavar M, Homayouni Tabrizi M. Synthesis and evaluation of biological effects of modified graphene oxidenanoparticles containing Lawson (Henna extract) on gastric cancer cells. Mol Biol Rep. 2023 Nov;50(11):8971-8983. https://doi.org/10.1007/s11033-023-08797-4
24. C.-Y. Huang, et al. (2017). A review on the effects of current chemotherapy drugs and natural agents in treating non–small cell lung cancer. *Biomedicine* **7** (4), 23.
25. R. Labianca, et al. (2007). The role of adjuvant chemotherapy in colon cancer. *Surgical oncology* **16**, 93–96.
26. A. S. Choudhari, et al. (2020). Phytochemicals in cancer treatment: From preclinical studies to clinical practice. *Frontiers in pharmacology* **10**, 1614.
27. C.-Z. Wang, et al. (2022). Effects of saffron and its active constituent crocin on cancer management: a narrative review. *Evaluation* **6**, 7.
28. N. Ghobadi and A. Asoodeh (2023). Co-administration of curcumin with other phytochemicals improves anticancer activity by regulating multiple molecular targets. *Phytotherapy Research* **37** (4), 1688–1702.
29. V. Aggarwal, et al. (2020). Molecular mechanisms of action of hesperidin in cancer: Recent trends and advancements. *Experimental Biology and Medicine* **245** (5), 486–497.
30. S. A. Al-Harbi, et al. (2021). Urolithins: The gut based polyphenol metabolites of ellagitannins in cancer prevention, a review. *Frontiers in Nutrition* **8**, 647582.
31. R. García-Villalba, et al. (2022). Urolithins: a comprehensive update on their metabolism, bioactivity, and associated gut microbiota. *Molecular Nutrition & Food Research* **66** (21), 2101019.
32. S. Mirzaei, et al. (2022). Urolithins increased anticancer effects of chemical drugs, ionizing radiation and hyperthermia on human esophageal carcinoma cells in vitro. *Tissue and Cell* **77**, 101846.
33. Z. Hafezi Ghahestani, et al. (2017). Evaluation of anti-cancer activity of PLGA nanoparticles containing crocetin. *Artificial cells, nanomedicine, and biotechnology* **45** (5), 955–960.
34. C. R. Dhas, et al. (2015). Visible light driven photocatalytic degradation of Rhodamine B and Direct Red using cobalt oxide nanoparticles. *Ceramics International* **41** (8), 9301–9313.
35. M. S. Islam, et al. (2017). Core–shell drug carrier from folate conjugated chitosan obtained from prawn shell for targeted doxorubicin delivery. *Journal of Materials Science: Materials in Medicine* **28**, 1–10.
36. P. Li, et al. (2011). Free radical-scavenging capacity, antioxidant activity and phenolic content of Pouzolzia zeylanica. *Journal of the Serbian Chemical Society* **76** (5), 709–717.
37. H. U. Hassan, et al. (2022). Comparative study of antimicrobial and antioxidant potential of olea ferruginea fruit extract and its mediated selenium nanoparticles. *Molecules* **27** (16), 5194.
38. R. Erenler, et al. (2021). Antioxidant activity of silver nanoparticles synthesized from Tagetes erecta L. leaves. *International Journal of Chemistry and Technology* **5** (2), 141–146.

39. K. B. Popova and R. Penchovsky (2024). General and specific cytotoxicity of chimeric antisense oligonucleotides in bacterial cells and human cell lines. *Antibiotics* **13** (2), 122.
40. Z. Sanaeimehr, I. Javadi, and F. Namvar (2018). Antiangiogenic and antiapoptotic effects of green-synthesized zinc oxide nanoparticles using Sargassum muticum algae extraction. *Cancer Nanotechnology* **9** (1), 3.
41. J. Stetefeld, S. A. McKenna, and T. R. Patel (2016). Dynamic light scattering: a practical guide and applications in biomedical sciences. *Biophysical reviews* **8** (4), 409–427.
42. P. Wongsa, P. Phatikulrungsun, and S. Prathumthong (2022). FT-IR characteristics, phenolic profiles and inhibitory potential against digestive enzymes of 25 herbal infusions. *Scientific Reports* **12** (1), 6631.
43. R. Singh, et al. (2015). Development and characterization of folate anchored Saquinavir entrapped PLGA nanoparticles for anti-tumor activity. *Drug development and industrial pharmacy* **41** (11), 1888–1901.
44. M. F. Queiroz, et al. (2014). Does the use of chitosan contribute to oxalate kidney stone formation? *Marine drugs* **13** (1), 141–158.
45. Z. Chen and D. Wu (2014). Monodisperse BSA-conjugated zinc oxide nanoparticles based fluorescence sensors for Cu2+ ions. *Sensors and Actuators B: Chemical* **192**, 83–91.
46. Y. Wang, et al. (2018). Superoxide dismutases: Dual roles in controlling ROS damage and regulating ROS signaling. *Journal of Cell Biology* **217** (6), 1915–1928.
47. A. Khan, et al. (2020). RNAi-Mediated silencing of catalase gene promotes apoptosis and impairs proliferation of bovine granulosa cells under heat stress. *Animals* **10** (6), 1060.
48. S. Senol, et al. (2015). Folate receptor α expression and significance in endometrioid endometrium carcinoma and endometrial hyperplasia. *International journal of clinical and experimental pathology* **8** (5), 5633.
49. M. Alirezaei, M. Ghobeh, and A. Es-haghi (2022). Poly (lactic-co-glycolic acid)(PLGA)-based nanoparticles modified with chitosan-folic acid to delivery of Artemisia vulgaris L. essential oil to HT-29 cancer cells. *Process Biochemistry* **121**, 207–215.
50. N. Ahmad, et al. (2020). A Chitosan-PLGA based catechin hydrate nanoparticles used in targeting of lungs and cancer treatment. *Saudi journal of biological sciences* **27** (9), 2344–2357.
51. M. G. Arafa, H. A. Mousa, and N. N. Afifi (2020). Preparation of PLGA-chitosan based nanocarriers for enhancing antibacterial effect of ciprofloxacin in root canal infection. *Drug Delivery* **27** (1), 26–39.
52. R. I. Teleanu, et al. (2019). Tumor angiogenesis and anti-angiogenic strategies for cancer treatment. *Journal of clinical medicine* **9** (1), 84.
53. M. Rajabi and S. A. Mousa (2017). The role of angiogenesis in cancer treatment. *Biomedicines* **5** (2), 34.
54. Snezhkina AV, Kudryavtseva AV, Kardymon OL, Savvateeva MV, Melnikova NV, Krasnov GS, Dmitriev AA. ROS Generation and Antioxidant Defense Systems in Normaland Malignant Cells. Oxid Med Cell Longev. 2019 Aug 5;2019:6175804. https://doi.org/10.1155/2019/6175804
55. A. C. Antony (1996). Folate receptors. *Annual review of nutrition* **16** (1), 501–521.
56. S. Gooneh-Farahani, M. R. Naimi-Jamal, and S. M. Naghib (2019). Stimuli-responsive graphene-incorporated multifunctional chitosan for drug delivery applications: a review. *Expert opinion on drug delivery* **16** (1), 79–99.
57. Marchetti C, Palaia I, Giorgini M, De Medici C, Iadarola R, Vertechy L, Domenici L, Di Donato V, Tomao F, Muzii L, Benedetti Panici P. Targeted drug delivery via folate receptors in recurrent ovarian cancer: a review. Onco Targets Ther. 2014 Jul 10;7:1223-36. https://doi.org/10.2147/OTT.S40947